PREDICTIVE CONTROL FOR A SINGLE-PHASE TO THREE-PHASE CONVERTER WITH TWO-PARALLEL SINGLE-PHASE RECTIFIERS

Ruben da Cruz Ferreira[1], Sofia M. Almeida Dias[1], Nady Rocha[1], Edison R. Cabral da Silva[1], Victor F. M. Bezerra Melo[2]

[1] Electrical Engineering Department, Federal University of Paraíba, Cidade Universitária, João Pessoa – PB, Brazil

[2] Renewable Energies Engineering Departament, Cidade Universitaria, João Pessoa – PB, Brazil

e-mail: ruben.ferreira@estudante.cear.ufpb.br, sofia.dias@alumni.cear.ufpb.br, nadyrocha@cear.ufpb.br, ercdasilva@gmail.com, victor@cear.ufpb.br

Abstract **– This paper presents a parallel single-phase to three-phase drive system, using two single-phase rectifiers. The rectifiers are not isolated from the grid by low-frequency transformers, so the reduction of the circulation current is an important objective for the control strategy. Modulated Model Predictive Control regulates the grid current and minimizes the circulation current between the parallel rectifiers. Furthermore, the analyzed predictive control consists of two strategies, where the first has the application of two vectors in a sampling period while the second has three vectors. The addition of a vector allows the reduction of the computational cost due to the reduction of tests performed in the predictive control and reduces the harmonic distortion in the electrical grid due to the greater application of vectors in a sampling period. Simulation and experimental results are presented in order to validate the control strategy.**

Keywords **– Single-Phase Grid, Parallel Converters, Modulated Model Predictive Control, Circulation Current, Three-Phase Induction Machine.**

I. INTRODUCTION

Three-phase motors have high efficiency, a smaller volume, and a smaller maintenance cost than their single-phase counterparts [1], [2]. If a three-phase grid is not available to provide power to the three-phase motor, a single-phase to three-phase converter can be used. Typical single-phase to three-phase converter applications can be found in remote and rural areas, residential heating, ventilation, and air conditioning (HVAC) systems.

A single-phase bridge rectifier and a three-phase inverter compose a basic bidirectional structure of a single-phase to three-phase converter, called a 5L-converter (five-leg converter). This topology employs five converter legs, totaling ten switches. In order to reduce the cost and size of power converters, several topologies have been proposed [2]–[6]. However, the proposed solutions present some disadvantages compared to the 5L-converter, such as the increase of the DC-link voltage, load voltage with constant frequency (normally equal to the grid), and increased harmonic distortion. The more interesting solution is a 3L-converter (three-leg converter) which has a shared leg between the single-phase input and the three-phase output of the converter [5], [6].

However, solutions that increase the number of switches can improve the quality of grid currents and load voltages. Despite increasing the number of switches, some solutions improve the efficiency of the power converter [7]–[12].

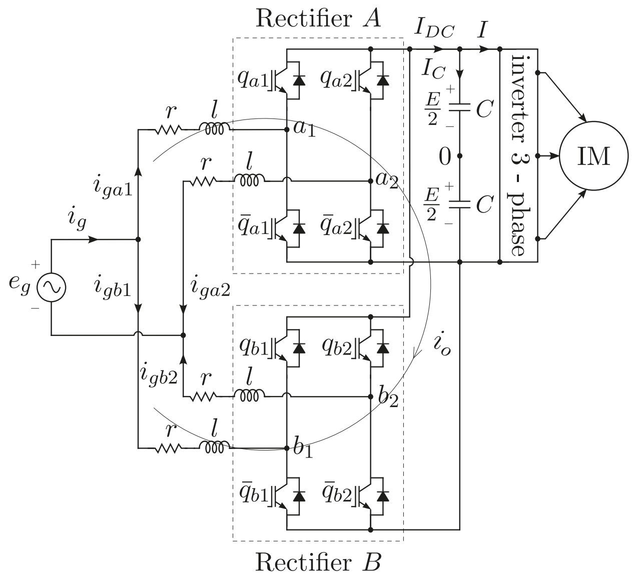

Fig. 1. Single-phase to three-phase AC-DC-AC converter with two parallel rectifiers proposed in [9].

The converter topology proposed in [12] uses a seven-level cascaded multilevel active rectifier and reduces the voltage rating of capacitors. However, three different dc-links and 12 converter legs are needed. An interesting solution is the topology presented in [9] (see Figure 1). The authors show that it is possible to increase the efficiency, reduce device current stress, and improve power quality at the single-phase side. Among the applications, this single-phase to three-phase converter can be highlighted by electric drive machines, generator systems, and electric railway tractions. In addition to the applications already mentioned above, single-phase parallel converters are widely used in uninterruptible power supply systems, power factor correction, and photovoltaic generation systems [8], [13].

Nonetheless, single-phase parallel converters without an isolation transformer lead to circulation currents between converters, increasing the current stress on the devices,

Manuscript received 06/29/2023; first revision 08/11/2023; accepted for publication 10/19/2023, by recommendation of Associate Editor Heverton Pereira. http://dx.doi.org/10.18618/REP.2023.4.0024.

increasing of power losses, and influencing the system's performance. Then reducing the circulation current is greatly important to obtaining the suiTable system performance [14].

Different control techniques have been proposed and studied in the technical literature. Among those applied to power electronics, the following stand out: linear control using a proportional and integral controller with pulse width modulation (PI-PWM), fuzzy control, sliding mode control, and predictive control. The Model Predictive Control (MPC) has drawn much attention in recent years. The MPC is a feedback control that uses the system model to predict the future behavior of the variables under control [15], [16]. Some MPC advantages are intuitive design, fast dynamic response, and the possibility of multiple control objectives [17], [18].

Due to its simplicity, the finite control set MPC (FCS-MPC) is the most popular MPC method. The FCS-MPC predicts the future behavior of the system based on the model and the finite number of possible switch positions of the power converter. The future switch positions are obtained by minimizing of cost function, next step the optimal switch position is directly applied without a modulation stage [19]–[23]. The FCS-MPC can be used for different systems, for example, [24] presents the use of FCS-MPC for control of DFIG-based wind power generation systems, [25] for a three-level neutral-point-clamped (NPC) converter, [26] five-phase and six-phase machine, etc.

The model-predictive pulse pattern control is the combination of MPC with Optimized pulse patterns (OPPs) [27]. Compared to FCS-MPC, the model-predictive pulse pattern control is much more complex [23]. Another method is the Optimal switching sequence MPC (OSS-MPC) [28]. It provides a fixed-switching frequency and has a better steady-state performance compared to FCS-MPC. Nonetheless, the computational effort and design controller are higher.

To mitigate the problem of variable switching frequency and maintain simplicity of design like in FCS-MPC, the Modulated Model Predictive Control (M^{2}PC) has been proposed [29]–[35]. The M^{2}PC is based on space vector modulation (SV-PWM). Unlike FS-MPC which uses a single vector in each sampling time, the M^{2}PC uses the same SV-PWM vector sequence. At each sampling time, all SV-PWM vector sequences are tested, and the duty cycle is calculated from the vector sequence that minimizes the cost function. Then, in the next sampling time, each vector of the SV-PWM sequence is applied to its respective duty cycle. Consequently, the M^{2}PC contributes to the performance of the system by improving power quality and lower harmonic distortion [33]–[35].

This paper discusses an AC-DC-AC single-phase to three-phase system with two rectifiers in parallel and the M^{2}PC control strategy previously presented in [36]. Two control strategies using the M^{2}PC are presented, which are based on the Space Vector Modulation (SVM), the first using a one-dimensional plane and the second using a vector plane. A comparison between the performance of the two strategies is discussed, as well as being compared with the FCS-MPC and the interleaved PWM strategy that was presented in [9]. These strategies define the best option for switching states to control the grid current with low harmonic distortion and minimize the circulation current. The simulation results were obtained using the PSIM® software. Also, experimental results validate the predictive control performance applied to the system. In summary, the main contributions of this paper compared with [36] are as follows:

I) Proposing a new strategy using the M^{2}PC based on the vector plan. In this way, it is possible to obtain a reduction in execution time of approximately 58.76% when compared with the strategy presented in [36];

II) Design to tune the gains of the Proportional-Integral (PI) based on a DC-link voltage controller;

III) Regarding the proposed strategy, due to redundant vector four different switching sequences were evaluated and compared;

IV) This article includes more simulation and experimental results, as well as a comparison among the strategies.

II. SYSTEM MODEL

As shown in Figure 1, the Parallel Rectifier (PR) system is composed of two full bridge single-phase converters (A and B) in parallel with four RL filters (r and l) and a DC-link. There is a three-phase inverter to supply a three-phase induction machine at the machine side.

According to Figure 1 the PR system equations are:

$$e_g = ri_{ga1} + l\frac{di_{ga1}}{dt} + ri_{ga2} + l\frac{di_{ga2}}{dt} + v_a \tag{1}$$

$$e_g = ri_{gb1} + l\frac{di_{gb1}}{dt} + ri_{gb2} + l\frac{di_{gb2}}{dt} + v_b \tag{2}$$

$$v_h = v_{h10} - v_{h20} \tag{3}$$

$$i_g = i_{ga1} + i_{gb1} \tag{4}$$

where e_g and i_g are, respectively, the voltage and current in the single-phase grid, i_{ga1}, i_{ga2}, i_{gb1} and i_{gb2} are, respectively, the current in the single-phase converters A and B, r, and l represent, in this order, the resistance and inductance of the RL filter, v_h is the rectifier voltage, v_{h10} and v_{h20} are the pole voltages of the converters, with $h = \{a,b\}$.

Due to the absence of an isolation transformer, circulation currents appear in converters A and B. From Figure 1, the model of the circulation current is:

$$-v_{a10} + v_{b10} = ri_{ga1} + l\frac{di_{ga1}}{dt} - ri_{gb1} - l\frac{di_{gb1}}{dt} \tag{5}$$

$$-v_{a20} + v_{b20} = -ri_{ga2} - l\frac{di_{ga2}}{dt} + ri_{gb2} + l\frac{di_{gb2}}{dt} \tag{6}$$

Adding (5) and (6), the following relationship is found:

$$v_o = 2ri_o + 2l\frac{di_o}{dt} \tag{7}$$

with

$$v_o = -v_{a10} - v_{a20} + v_{b10} + v_{b20} \tag{8}$$

$$i_{o1} = i_{ga1} - i_{ga2} \tag{9}$$

$$i_{o2} = i_{gb1} - i_{gb2} \tag{10}$$

$$i_o = i_{o1} = -i_{o2}. \tag{11}$$

From (1), (2), (5), (9) and (10), the system model is:

$$e_g = 2ri_{ga1} + 2l\frac{di_{ga1}}{dt} - \frac{v_o}{2} + v_a \tag{12}$$

$$e_g = 2ri_{gb1} + 2l\frac{di_{gb1}}{dt} + \frac{v_o}{2} + v_b \tag{13}$$

The equivalent model is obtained from (12) and (13), that is:

$$e_g = ri_g + l\frac{di_g}{dt} + v_g \tag{14}$$

$$v_g = \frac{v_a + v_b}{2} \tag{15}$$

The voltages v_a, v_b and v_o depend on the switching state of the converters and the DC-link voltage, and can be rewritten as:

$$v_a = (q_{a1} - q_{a2})E \tag{16}$$

$$v_b = (q_{b1} - q_{b2})E \tag{17}$$

$$v_o = (-q_{a1} - q_{a2} + q_{b1} + q_{b2})E \tag{18}$$

where q_{a1}, q_{a2}, q_{b1}, and q_{b2} are the switching states of the converters A and B, and E is the DC-link voltage.

Table I shows the relationship between the switching states of converters A and B and the voltages v_a, v_b, v_g and v_o. In addition, the voltages v_g and v_o have five voltage levels being, respectively, $[-E, -E/2, 0, E/2, E]$ and $[-2E, -E, 0, E, 2E]$.

TABLE I
Switching States and Resulting Voltages

$\vec{v}$	q_{a1}	q_{a2}	q_{b1}	q_{b2}	v_a	v_b	v_g	v_o
V_0	0	0	0	0	0	0	0	0
V_1	0	0	0	1	0	$-E$	$-E/2$	E
V_2	0	0	1	0	0	E	$E/2$	E
V_3	0	0	1	1	0	0	0	$2E$
V_4	0	1	0	0	$-E$	0	$-E/2$	$-E$
V_5	0	1	0	1	$-E$	$-E$	$-E$	0
V_6	0	1	1	0	$-E$	E	0	0
V_7	0	1	1	1	$-E$	0	$-E/2$	E
V_8	1	0	0	0	E	0	$E/2$	$-E$
V_9	1	0	0	1	E	$-E$	0	0
V_{10}	1	0	1	0	E	E	E	0
V_{11}	1	0	1	1	E	0	$E/2$	E
V_{12}	1	1	0	0	0	0	0	$-2E$
V_{13}	1	1	0	1	0	$-E$	$-E/2$	$-E$
V_{14}	1	1	1	0	0	E	$E/2$	$-E$
V_{15}	1	1	1	1	0	0	0	0

III. DISCRETE MODEL

The development of the prediction of i_{ga1}, i_{gb1}, i_o can be done with state space equation using (12), (13) and (7), i.e.:

$$\dot{x}(t) = Mx(t) + Nu(t) \tag{19}$$

where $x(t) = [i_{ga1}(t)\ i_{gb1}(t)\ i_o(t)]^T$, $u(t) = [(e_g(t) + v_o/2 - v_a(t))\ (e_g(t) - v_o/2 - v_b(t))\ v_o(t)]^T$ and matrices M and N, being, respectively:

$$M = \begin{bmatrix} -\frac{r}{l} & 0 & 0 \\ 0 & -\frac{r}{l} & 0 \\ 0 & 0 & -\frac{r}{l} \end{bmatrix} \text{ and } N = \begin{bmatrix} \frac{1}{2l} & 0 & 0 \\ 0 & \frac{1}{2l} & 0 \\ 0 & 0 & \frac{1}{2l} \end{bmatrix}.$$

The prediction proposed for currents is performed using the rectangular direct discretization method [37], defined as:

$$x_{k+1} = (I + MT_s)x_k + NT_s u_k \tag{20}$$

where k represents the discrete instant of time; consequently, $(k+1)$ is a step forward, I is the identity matrix with a dimension equal to that of M and N, T_s is the sampling time and x_k and u_k are, respectively, discrete $x(t)$ and $u(t)$.

In order to prevent a computational delay, present in the experimental process, it is necessary to establish the prediction in the step $(k+2)$ to compensate for the delay and, consequently, apply in $(k+1)$ the predicted switching state [29], [32], [36], [38], [39]. In this case, assuming that $e_g(k+1) = e_g(k)$ for a small sampling time T_s.

Using (20) to calculate the currents in the first horizon, the currents at the instant $(k+2)$ can be predicted as:

$$x_{k+2} = (I + MT_s)x_{k+1} + NT_s u_{k+1}. \tag{21}$$

IV. CONTROL STRATEGY

This paper presents two strategies to define the switching states. Strategy I is based on a single-dimensional control region and a set of pairs of adjacent vectors are considered to define switch states, while Strategy II is based on the plan v_g and v_o and a set of three adjacent vectors are used to improve the performance of the parallel rectifier. Figure 2 shows the block diagram implementation of the M^{2}PC to parallel single-phase rectifier. The amplitude I_g^* is given from the error between the DC-link voltage reference (E^*) and the measured DC-link voltage (E) using a Proportional-Integral (PI) controller. The reference current of the electrical grid is used with two horizons, i.e., $i_g^* = i_g^*(k+2)$. The control block R_i is responsible for obtaining the reference current and estimating its value to the second horizon. A Phase-Locked Loop (PLL) scheme has been used to obtain a high power factor, i.e., voltage and current in the grid are in phase [40].

The system model provides x_k and u_k in which they become input to the discrete model and, in turn, return the prediction of currents x_{k+2} to be used in the total cost function. Therefore, the M^{2}PC is used to minimize the cost function, that is, defining the best option of vectors and their duty cycles.

A. Design of the Dc-Link Voltage

Figure 3 presents the block diagram of the DC-link voltage control strategy. For the DC-link voltage gain design, the inner predictive current control loop is neglected because it has a faster control loop dynamic than the outer DC-link voltage control loop.

According to [41], the gain D can be deduced from the power balance between the AC- and DC-side of the rectifier, that is, $P_{DC} = EI_{DC}$ is approximately equal to $P_{AC} = 0.5E_gI_g$ (where E_g is the magnitude of grid voltage). Also, considering that the ripple voltage for DC-link is small compared with the reference value, then it's possible to approximate the DC-link voltage with its reference, i.e., $P_{DC} \approx E^*I_{DC}$ the same can be used for grid current, i.e., $P_{AC} \approx 0.5E_gI_g^*$, with this:

$$E^*I_{DC} \approx 0.5E_gI_g^* \tag{22}$$

From Figure 3 and (22), the gain D is written as follows:

$$D = \frac{I_{DC}}{I_g^*} = 0.5\frac{E_g}{E^*} \tag{23}$$

From Figure 3, the closed-loop system transfer function, for current I equal to 0, is given by:

$$\frac{E}{E^*} = \frac{\frac{Dk_p}{C'}s + \frac{Dk_i}{C'}}{s^2 + \frac{Dk_p}{C'}s + \frac{Dk_i}{C'}} \tag{24}$$

where $C' = C/2$ is the equivalent capacitance of the DC-link. Comparing the denominator of (24) with the characteristic equation, the gains are given by:

$$k_p = \frac{2C'\zeta\omega_c}{D} \tag{25}$$

$$k_i = \frac{C'\omega_c^2}{D} \tag{26}$$

where ζ is the appropriate damping ratio and ω_c is the natural frequency of oscillation.

B. Strategy I

In this strategy, the M^{2}PC is based on the Space Vector Modulation (SVM) for a single-phase converter and was implemented using a single-dimensional control region [32], [42]. The SVM allows a set of pairs of adjacent vectors to be considered for the application of the control strategy. The voltage levels are distributed among four sectors (I, II, III, IV) as shown in Figure 4, where sectors are based on the v_g voltage. Note that the voltage levels $-E/2$, 0, and $E/2$ have redundant vectors. The set of adjacent vector pairs (based on v_g) for the sectors presents 56 possible combinations. For predictive control, a large number of switching possible increases the computational burden leading to a reduction in sampling time, which is an undesirable solution for power electronics applications.

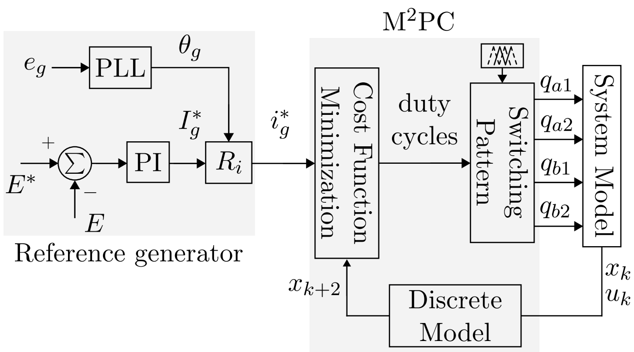

Fig. 2. Control diagram of the rectifier side using the M^{2}PC method.

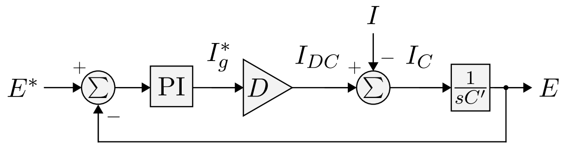

Fig. 3. Diagram for DC-link voltage controller.

A simple solution, that reduces the computational burden, is to select voltage vectors that eliminate the circulating current, for instance, using the pair of vectors $0000-0101$ and $0000-1010$ to rectifier control. However, in this solution, the v_g voltage has only a three-level voltage, i.e., $[-E, 0, E]$. To reduce the number of switching combinations and obtain the v_g voltage with five levels, only 16 different pairs of adjacent vectors are applied. The vector pairs are selected when there is only a single switching change and the null vectors 1100 and 0011 are not used because they have a greater impact on the circulation current, as shown in Table I. Table II shows the vector pairs of adjacent vectors that have been used.

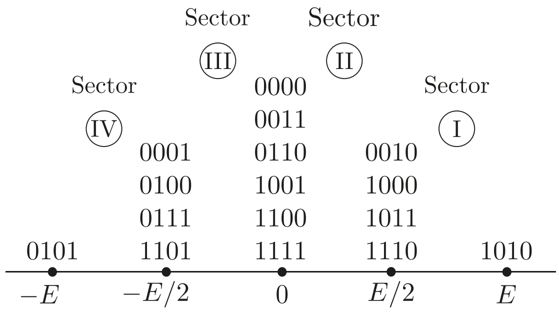

Fig. 4. Single-dimensional control region for v_g voltage.

TABLE II
Selected Adjacent Vectors

Sector I	Sector II	Sector III	Sector IV
1000-1010	0000-0010	0001-0000	0101-0001
0010-1010	0000-1000	0100-0000	0101-0100
1110-1010	1111-1110	1101-1111	0101-0111
1011-1010	1111-1011	0111-1111	0101-1101

As the M^{2}PC tests two adjacent vectors in each sampling cycle, the cost function is calculated for each vector. See [36] for more details on the cost function and calculation of duty cycles. After obtaining the duty cycles, the switching states are obtained by comparing the duty cycle with two high-frequency triangular carrier signals. The phase shift of the triangular carrier between the rectifiers is 180°.

Figure 5 shows the flowchart for the operation of M^{2}PC operating in the PR, where δ is the number of iterations. For Strategy I, δ is equal to 16. The overall control procedure can be summarized as:

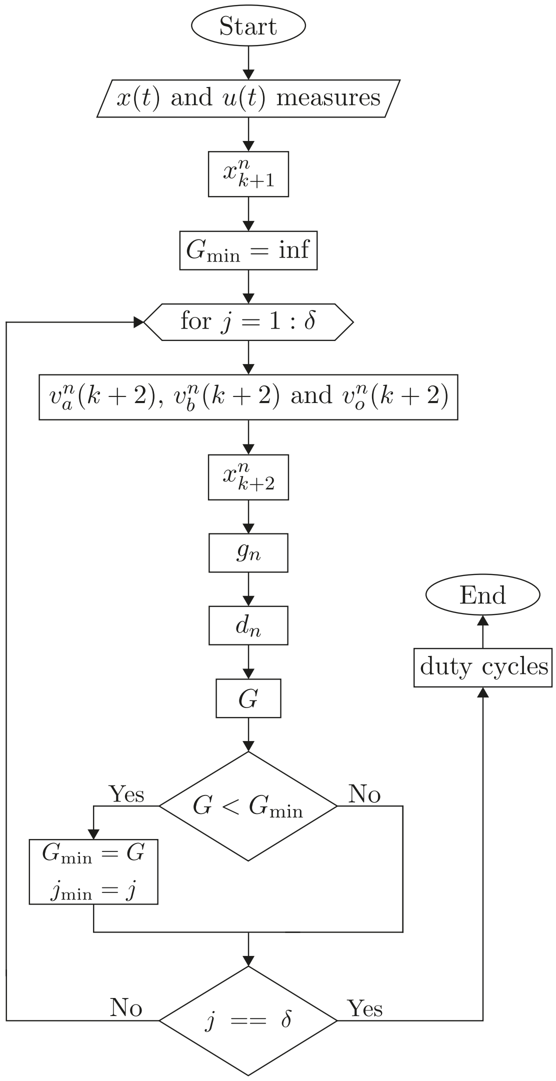

Fig. 5. Flowchart for M^{2}PC applied to PR.

1. Sampling $i_{ga1}(k)$, $i_{ga2}(k)$, $i_{gb1}(k)$, $e_g(k)$ and $E(k)$;
2. Apply the optimal duty-cycle and calculated $v_a(k)$, $v_b(k)$ and $v_o(k)$;
3. Predict the x_{k+1} variables, i.e., $i_{ga1}(k+1)$, $i_{ga2}(k+1)$ and $i_o(k+1)$ using (20);
4. Definition of $G_{\min} = \texttt{inf}$;
5. Structure in the `for` loop:
   (a) Evaluate the predicted x_{k+2}, i.e., the currents $i_{ga1}(k+2)$, $i_{ga2}(k+2)$ and $i_o(k+2)$ from (21);
   (b) Calculate the cost function for each voltage vector;
   (c) Calculate the duty cycles;
   (d) Select the vectors that optimize the total cost function.
6. Definition of duty cycles obtained with M^{2}PC.

C. Strategy II

This strategy is based on the plan v_g and v_o, where v_g is the real axis and v_o is the imaginary axis. There are 16 switching states, and the parallel single-phase rectifier generates v_g with five levels. The $v_g \times v_o$ plan is composed of nine vectors, eight active vectors, and one null vector.

Figure 6 shows that the voltage plan can be distributed among eight sectors, but the selected sectors do not contain the $-2E$ and $2E$ components of the voltage v_o.

Table III shows the possibilities of vectors (V_x, V_y and V_z) for each sector. For example, for option IIa in sector I: $V_x = V_{14}$, $V_y = V_{10}$ and $V_z = V_{11}$. The three vectors are selected to reduce the number of switch commutations in each sector, reducing the switching losses. A restriction of the parallel rectifier is to obtain equal voltages or the same average voltage between the converters. In this way, there are at least four possibilities to define the vectors applied in the modulation of the parallel rectifiers, that is:

IIa: Legs a_1 and b_1 at low switching frequency and a_2 and b_2 at high switching frequency;

IIb: Legs a_2 and b_2 at low switching frequency and a_1 and b_1 at high switching frequency;

IIc: Sectors I and II with a_1 and b_1 at high switching frequency and sectors III and IV with a_2 and b_2 at high switching frequency;

IId: Sectors I and II with a_2 and b_2 at high switching frequency and sectors III and IV with a_1 and b_1 at high switching frequency.

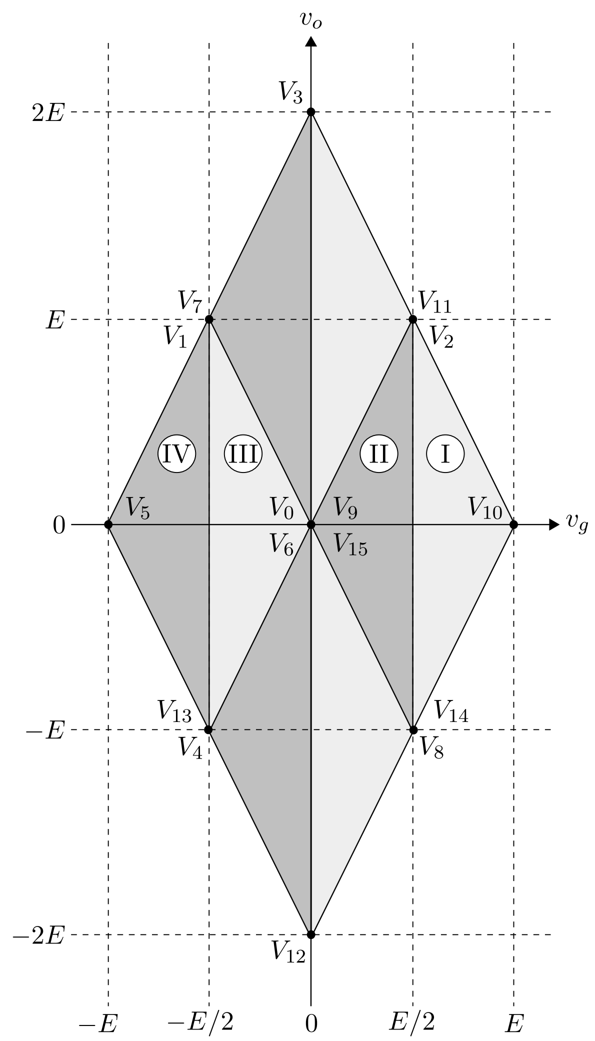

Fig. 6. Plan $v_g \times v_o$ control region.

Options IIa and IIb make one of the legs operate at a low switching frequency while the other legs operate at a high switching frequency. Options IIc and IId make the legs operate half of the cycle at a low switching frequency and the other half of the cycle at a high switching frequency. These options maintain the voltage levels as shown in Table I.

In this strategy, three vectors are applied in the sampling time interval and the cost function is calculated for each vector. In this way, the cost function is:

$$g_n = \left[i_g^*(k_2) - i_g^n(k_2)\right]^2 + \lambda_o \left[i_o^*(k_2) - i_o^n(k_2)\right]^2 \tag{27}$$

where $k_2 = k+2$, $n = \{x, y, z\}$ indicating the analyzed vector, $i_g(k+2) = i_{ga1}(k+2) + i_{gb1}(k+2)$ and λ_o is the weighting factor of the circulation current. The duty cycles corresponding to each vector is:

$$d_x = \frac{g_y g_z}{g_x g_y + g_x g_z + g_y g_z} \tag{28}$$

$$d_y = \frac{g_x g_z}{g_x g_y + g_x g_z + g_y g_z} \tag{29}$$

$$d_z = \frac{g_x g_y}{g_x g_y + g_x g_z + g_y g_z} \tag{30}$$

In this way, the selected vectors are those that provide the smallest value of the total cost function:

$$G = d_x g_x + d_y g_y + d_z g_z \tag{31}$$

The M^2PC operating processes for Strategy II are the same used in Strategy I, that is, the steps shown in the flowchart in the Figure 5, but with δ equal to 4. In the same way as Strategy I, the switching states are obtained by comparing the duty cycle with two high-frequency triangular carrier signals with a phase shift of 180° for each one of the rectifiers.

TABLE III
Vector Set to Strategy II

Option	Sector I	Sector II	Sector III	Sector IV
IIa	V_{14}-V_{10}-V_{11}	V_{14}-V_{15}-V_{11}	V_4-V_0-V_1	V_4-V_5-V_1
IIb	V_8-V_{10}-V_2	V_8-V_0-V_2	V_{13}-V_{15}-V_7	V_{13}-V_5-V_7
IIc	V_{14}-V_{10}-V_{11}	V_{14}-V_{15}-V_{11}	V_{13}-V_{15}-V_7	V_{13}-V_5-V_7
IId	V_8-V_{10}-V_2	V_8-V_0-V_2	V_4-V_0-V_1	V_4-V_5-V_1

TABLE IV
Execution Time of Strategies

	Tests for execution time				
Strategy	1	2	3	4	5
I	1.195 s	1.204 s	1.192 s	1.235 s	1.197 s
II	0.494 s	0.493 s	0.492 s	0.506 s	0.499 s

Due to the use of three vectors, it is possible to reduce the number of tests by 50% in relation to Strategy I, since it is necessary to evaluate only the eight sectors shown in Figure 6. However, due to the elimination of the levels with the highest voltage magnitude v_o, there is a reduction from eight to four sectors. Because of that, the M^2PC needs to carry out only four tests to define the duty cycles for the vectors. Despite increasing the number of calculations performed in the cost function when compared to Strategy I, there is a reduction from sixteen to four tests, that is, a 75% reduction in iterations. Using the `profiler` function of MATLAB®, it is possible to compare the execution time between the codes used in Strategies I and II. The `profiler function` is a performance analysis by measuring the execution time of code segments, providing detailed time information for each part of the code. Table IV shows the execution time of codes for Strategies I and II, using the `profiler function`. For each strategy, the execution time was calculated five times ensuring greater accuracy of results. The average time for Strategies I and II are, respectively, 1.205 s and 0.497 s. Thus, comparing average values, it was noted that Strategy II obtained a reduction in execution time of approximately 58.76% in relation to Strategy I. Also, the use of three vectors provides a reduction of Total Harmonic Distortion (THD) since more vectors are applied in each sampling interval T_s.

V. SIMULATION RESULTS

To demonstrate the feasibility of the rectifier with parallel converters using predictive control, digital simulations have been performed in PSIM® software. The results for the two strategies were obtained for the following conditions: the voltage in the electrical grid equal to 110 V (RMS)/60 Hz, RL filter $r = 0.2\ \Omega$ and $l = 6$ mH, DC-link reference voltage E^* equal to 200 V, capacitance C of DC-link is equal to 2200 μF, the switching frequency equal to 10 kHz, the sampling period T_s equal to 50 μs, the gains of the PI controller were $k_p = 0.0385$ and $k_i = 0.3773$ ($\zeta = 0.59$ and $\omega_c = 11.55$), weighting factor equal to 0.25 for both strategies. At the load side, a three-phase RL load has been used instead of a three-phase machine using a reference current equal to 2 A/20 Hz.

A. Results Simulation for Strategy I

The results obtained for Strategy I are shown in Figures 7, 8, and 9. Figure 7.a shows grid current and voltage results. Notice that the grid voltage and current waveforms are in phase, obtaining a high power factor. According to Figure 7.b, the current in the electrical grid followed its reference and obtained a THD of 2.91%. Figure 7.c shows sinusoidal three-phase load currents with a frequency of 20 Hz. From Figure 7.d, note that the vectors minimize the circulation current, with Root Mean Square (RMS) equal to 0.19 A.

Internal currents of the rectifiers, shown in Figures 8.a and 8.b, with THD of i_{ga1}, i_{ga2}, i_{gb1} and i_{gb2} equal to 3.32%, 14.14%, 3.32% and 14.13%, respectively. The DC-link voltage under control at 200 V is shown in Figure 8.c. This voltage presents a second-order harmonic due to the single-phase grid connection. According to Figure 8.d, the voltage v_o did not exceed voltage levels $-E$ and E. As shown in Figure 9.a, v_g has a five-level waveform.

Voltage waveforms for the rectifiers are shown in Figures 9.b, 9.c and 9.d. Therefore, it is noted that the legs a_1 and b_1 are operating at low switching frequency while legs a_2 and b_2 are at high switching frequency, but the voltages v_a and v_b get the expected voltage levels, that is, three levels.

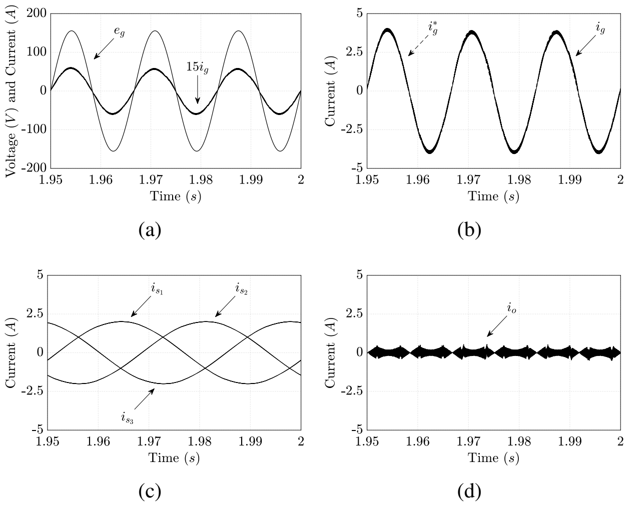

Fig. 7. Simulation results for Strategy I. (a) Voltage and current of the grid, e_g and i_g. (b) Grid current and reference, i_g and i_g^*. (c) Load currents i_{s1}, i_{s2} and i_{s3}. (d) Circulation current.

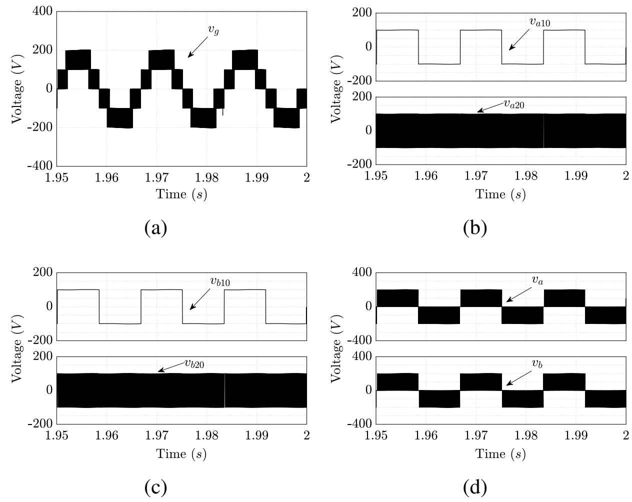

Fig. 9. Simulation results for Strategy I. (a) Voltage, v_g. (b) Pole voltages v_{a10} and v_{a20}. (c) Pole voltages v_{b10} and v_{b20}. (d) Voltage of the rectifiers v_a and v_b.

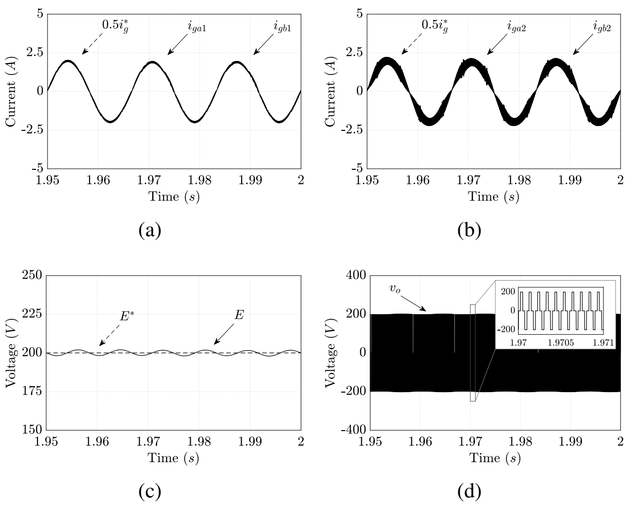

Fig. 8. Simulation results for Strategy I. (a) Currents i_{ga1}, i_{gb1} and references. (b) Currents i_{ga2}, i_{gb2} and references. (c) DC-link voltage and reference, E and E^*. (d) Voltage v_o.

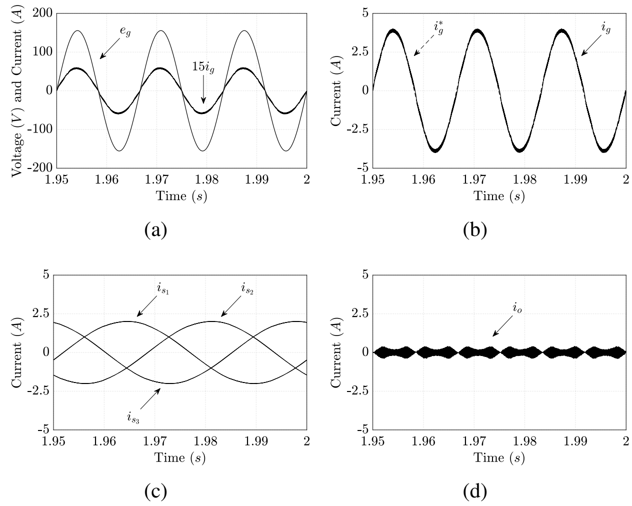

Fig. 10. Simulation results for the Strategy IIa. (a) Current and voltage of the grid, e_g and i_g. (b) Grid current and reference, i_g and i_g^*. (c) Load currents i_{s1}, i_{s2} and i_{s3}. (d) Circulation current i_o.

B. Results Simulation for Strategy II

The presented results of Strategy II are summarized with option IIa, except for the pole voltages.

The results of the system, using four regions of the vector plane to the M^{2}PC with the Strategy IIa are shown in Figures 10, 11 and 12. Figure 10.a shows that the grid current and voltage are in the same phase, i.e., with a high power factor. According to Figure 10.b, the current in the electrical grid followed its reference and obtained a THD of 2.64%. Figure 10.c shows sinusoidal three-phase load currents with a frequency of 20 Hz. From Figure 10.d note that the vectors minimize the circulation current, with RMS value equal to 0.19 A. The internal currents of the rectifiers, shown in Figures 11.a and 11.b, with THD of i_{ga1}, i_{ga2}, i_{gb1} and i_{gb2} equal to 2.61%, 13.78%, 2.61% and 13.82%, respectively. The DC-link voltage is under control at 200 V as shown in Figure 11.c. According to the Figure 11.d, the voltage v_o did not exceed the selected voltage levels, i.e., $-E$ and E levels and, as shown in Figure 12.a, the v_g voltage has a five-level waveform.

The rectifier voltages for Strategies IIa, IIb, IIc, and IId are shown in Figures 12, 13, 14 and 15, respectively. In Figure 12 is noted that legs a_1 and b_1 are operating at low switching frequency while legs a_2 and b_2 are at high frequency (equal to Strategy I) and in the Figure 13 the opposite situation. In Figures 14 and 15 it is noted that the legs operate at low switching frequency only in a half-cycle. In all cases, the voltages v_a and v_b get the expected voltage levels, that is, three levels. Thus, it can be seen that the results between strategies I and II are similar. However, Strategy II has a better THD since three vectors are used in each sampling period instead of the two vectors applied in Strategy I.

C. Comparison of Results Between Strategies

In order to compare the results, in this section, Strategy I and Strategy II are compared with the traditional PWM (Pulse

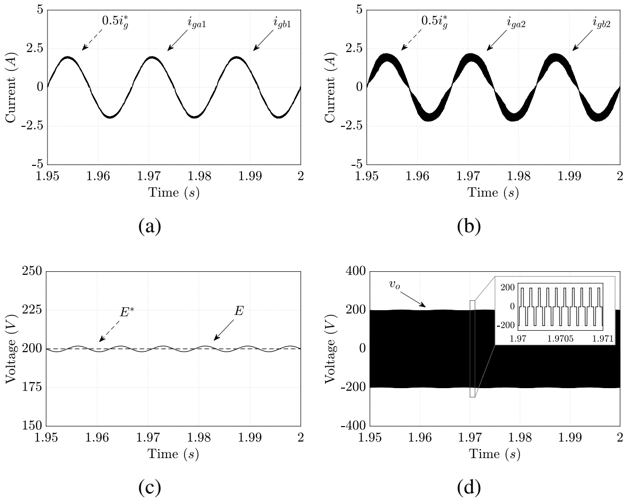

Fig. 11. Simulation results for the Strategy IIa. (a) Currents i_{ga1}, i_{gb1} and references. (b) Currents i_{ga2}, i_{gb2} and references. (c) DC-link voltage and reference, E and E^*. (d) Voltage v_o.

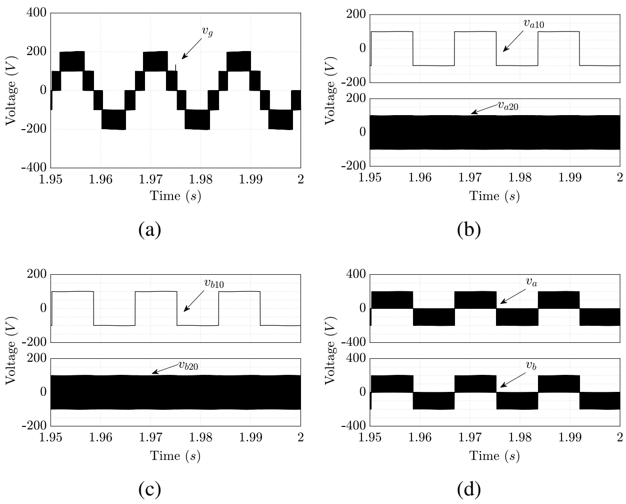

Fig. 12. Simulation results for the Strategy IIa. (a) Voltage, v_g. (b) Pole voltages v_{a10} and v_{a20}. (c) Pole voltages v_{b10} and v_{b20}. (d) Voltage of the rectifiers v_a and v_b.

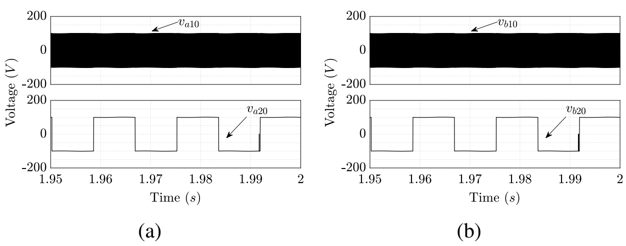

Fig. 13. Simulation results for the Strategy IIb. (a) Pole voltages v_{a10} and v_{a20}. (b) Pole voltages v_{b10} and v_{b20}.

Width Modulation) strategy using a linear PI controller. The control strategy using the PWM strategy was presented in [9]. Table V shows the results obtained for the PWM Strategy, Finite Control Set-Model Predictive Control (FCS-MPC), and M^{2}PC strategies I, IIa, and IIc. The results were obtained with the same conditions, with a switching frequency equal

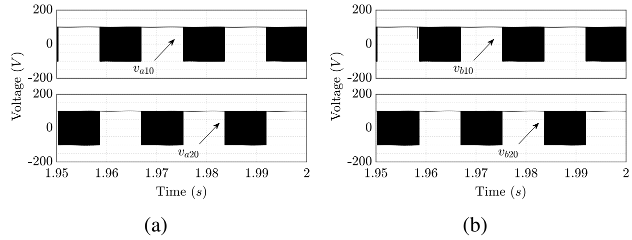

Fig. 14. Simulation results for the Strategy IIc. (a) Pole voltages v_{a10} and v_{a20}. (b) Pole voltages v_{b10} and v_{b20}.

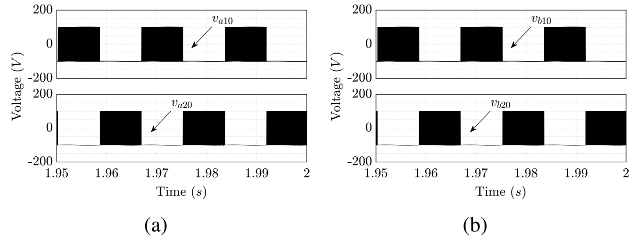

Fig. 15. Simulation results for the Strategy IIc. (a) Pole voltages v_{a10} and v_{a20}. (b) Pole voltages v_{b10} and v_{b20}.

to 10 kHz, and the sampling period T_s equal to 50 μs,

TABLE V
Comparison of THD Between Strategies

	PWM	FCS-MPC	M^{2}PC - I	M^{2}PC - IIa	M^{2}PC - IIc
i_g	2.79%	6.94%	3.32%	2.61%	2.69%
i_{ga1}	9.99%	6.94%	3.32%	2.61%	10.17%
i_{ga2}	10.14%	23.99%	14.14%	13.78%	10.19%
i_{gb1}	10.06%	6.94%	3.32%	2.61%	10.15%
i_{gb2}	10.69%	25.01%	14.13%	13.82%	10.17%

The grid current using FCS-MPC showed a high THD between strategies because only one voltage vector is applied during each sampling period. The strategy I presents higher harmonic distortion values than the PWM Strategy because it uses only a pair of adjacent vectors in each sampling period. Furthermore, Strategies II (IIa and IIc) present the lowest harmonic distortion values. To Strategy IIa, the THD grid current is reduced in 7%, 62%, and 21% when compared with the PWM strategy, FCS-MPC, and Strategy I, leading to a better quality of the grid's current performance. On the other hand, the THD of internal currents depends on the PWM strategy. Comparing the PWM Strategy with Strategy IIc, note that they have a low difference of THD in the internal currents but with an improvement in the grid current using Strategy IIc.

Table VI shows the RMS value of circulation currents. A similar result has been obtained with all strategies, with a little reduction in RMS value when Strategies II and I were used.

VI. EXPERIMENTAL RESULTS

The effectiveness of the proposed M^{2}PC strategy is validated in the laboratory. However, only the parallel rectifier was implemented. The experimental setup is based on a Digital Signal Processor (DSP) TMS320F28335 with a microcomputer equipped with appropriate plugin boards and

TABLE VI
Comparison of RMS Between Strategies

	PWM	FCS-MPC	M^2PC - I	M^2PC - IIa	M^2PC - IIc
i_o	0.20 A	0.32 A	0.19 A	0.19 A	0.19 A

sensors, as shown in Figure 16. The results were obtained by oscilloscope Agilent DSO-X 3014A 100 MHz. The switching frequency was equal to 10 kHz, the DC-link voltage was equal to 200 V, and capacitance C of DC-link was equal to 2200 μF. A load of 100 Ω was used. The RL filter has the following parameters: resistance $r = 0.75$ Ω and inductance $l = 10.5$ mH. The voltage in the single-phase grid was equal to 110 V (RMS) and 60 Hz fundamental frequency. The sampling period, gains of the PI controller, and weighting factor are the same as those used in the simulation.

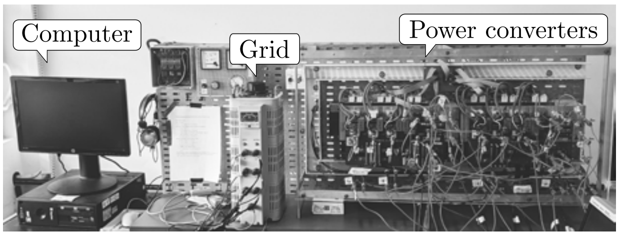

Fig. 16. Experimental setup.

The experimental results were obtained using Strategy IIa. Figure 17.a show sinusoidal grid current and DC-link voltage equal to 200 V. As the grid voltage and current are in phase, a high power factor is obtained. As shown in Figure 17.b, the rectifier voltages have three levels and the v_g voltage has five levels. Figures 17.c and 17.d show the internal rectifier currents, showing that the circulation current is almost zero. According to Figures 17.e and 17.f, pole voltages v_{a10} and v_{b10} are at low switching frequency while voltages v_{a20} and v_{b20} are at high switching frequency, characteristic behavior of Strategy IIa.

In addition, a load transient was performed with a 25% increase in load. Figures 18.a and 18.b show the behavior of the system with the load transient. The DC-link returns to its reference value after a small drop and the circulation current remains with practically null value. All experimental results are in full accordance with the simulation results presented. Furthermore, the experimental results show that the proposed strategy is able to achieve the goals: sinusoidal grid current, mitigate of circulation current, and v_g with five-level voltage.

VII. CONCLUSIONS

A single-phase to three-phase converter using Modulated Model Predictive Control was presented in this work. The converter consists of two parallel single-phase rectifiers without isolation transformers and a three-phase inverter. Two strategies using M^2PC were presented, which provided a sinusoidal grid current with a high power factor and reduction of the circulation current between the parallel rectifiers. For both strategies, an RMS value for circulation current equal to 0.19 A was obtained. Among the strategies discussed, Strategy II performed better compared to Strategy I since it enabled a reduction in computational cost by 58.68% and better THD in the electrical grid. Strategy IIa and IIc obtained, respectively, THD equal to 2.61% and 2.69% while for Strategy I it was obtained 3.32%. The improvement presented by Strategy II regarding the computational cost occurs due to the reduction of iterations to obtain the best set of vectors and, about the THD, occurs due to the increase of vectors applied in a sampling period.

ACKNOWLEDGEMENTS

The authors would like to thank in part the Coordenação de Aperfeiçoamento de Pessoal de Nível Superior – Brasil (CAPES) and the Conselho Nacional de Desenvolvimento Científico e Tecnológico (CNPq) for the financial support.

REFERENCES

[1] A. Gonzalez, C. Hernandez, M. A. Arjona, "A Novel High-Efficiency Parallel-Winding Connection for a Three-Phase Induction Motor Fed by a Single-Phase Power Supply", *IEEE Transactions on Energy Conversion*, vol. 29, no. 2, pp. 269–277, Jun. 2014, doi: 10.1109/TEC.2014.2305755.

[2] D.-C. Lee, Y.-S. Kim, "Control of Single-Phase-to-Three-Phase AC/DC/AC PWM Converters for Induction Motor Drives", *IEEE Transactions on Industrial Electronics*, vol. 54, no. 2, pp. 797–804, Apr. 2007, doi:10.1109/TIE.2007.891780.

[3] S. A. O. da Silva, F. A. Negrão, "Single-Phase to Three-Phase Unified Power Quality Conditioner Applied in Single-Wire Earth Return Electric Power Distribution Grids", *IEEE Transactions on Power Electronics*, vol. 33, no. 5, pp. 3950–3960, May 2018, doi:10.1109/TPEL.2017.2723573.

[4] P. Enjeti, A. Rahman, R. Jakkli, "Economic single-phase to three-phase converter topologies for fixed and variable frequency output", *IEEE Transactions on Power Electronics*, vol. 8, no. 3, pp. 329–335, Jul. 1993, doi:10.1109/63.233290.

[5] P. Enjeti, A. Rahman, "A new single-phase to three-phase converter with active input current shaping for low cost AC motor drives", *IEEE Transactions on Industry Applications*, vol. 29, no. 4, pp. 806–813, Jul.–Aug. 1993, doi:10.1109/28.231999.

[6] C. B. Jacobina, E. C. dos Santos, M. B. d. R. Correa, E. R. C. da Silva, "Single-Phase-Input Reduced-Switch-Count AC–AC Drive Systems", *IEEE Transactions on Industry Applications*, vol. 44, no. 3, pp. 789–798, May–Jun. 2008, doi:10.1109/TIA.2008.921420.

[7] C. B. Jacobina, E. C. dos Santos, N. Rocha, B. de Sá Gouveia, E. R. C. da Silva, "Reversible AC Drive Systems Based on Parallel AC–AC DC-Link Converters", *IEEE Transactions on Industry Applications*, vol. 46, no. 4, pp. 1456–1467, Jul.–Aug. 2010, doi:10.1109/TIA.2010.2049724.

[8] Y. Xia, M. Yu, Y. Zhang, Z. Lv, W. Wei, "Decentralized Suppression Strategy of Circulating Currents Among IPOP Single-Phase DC/AC Converters", *IEEE Journal of Emerging and Selected Topics in Power Electronics*,

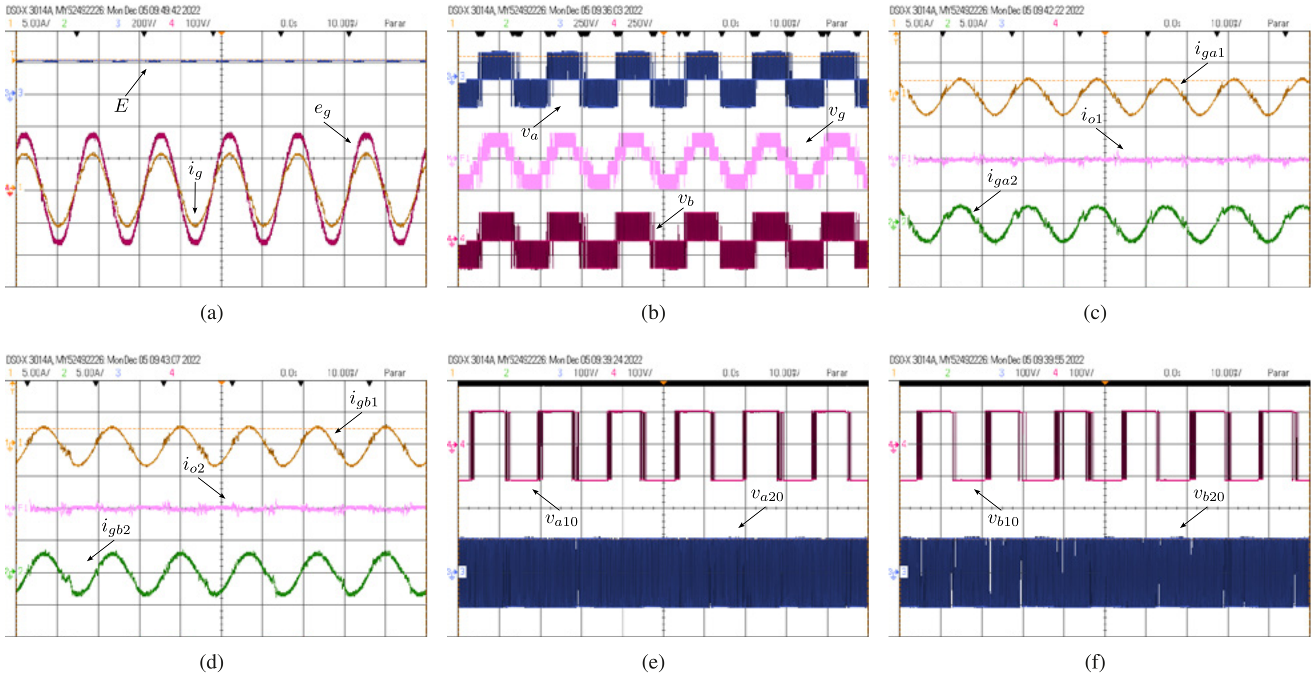

Fig. 17. Experimental results. (a) DC-link voltage E, voltage and current of grid e_g and i_g. (b) Voltages of the parallel rectifiers, v_a, v_b and v_g. (c) Currents of the rectifier A, $i_{g_{a1}}$, $i_{g_{a2}}$ and i_{o1}. (d) Currents of the rectifier B, $i_{g_{b1}}$, $i_{g_{b2}}$ and i_{o2}. (e) Pole voltages v_{a10} and v_{a20}. (f) Pole voltages v_{b10} and v_{b20}.

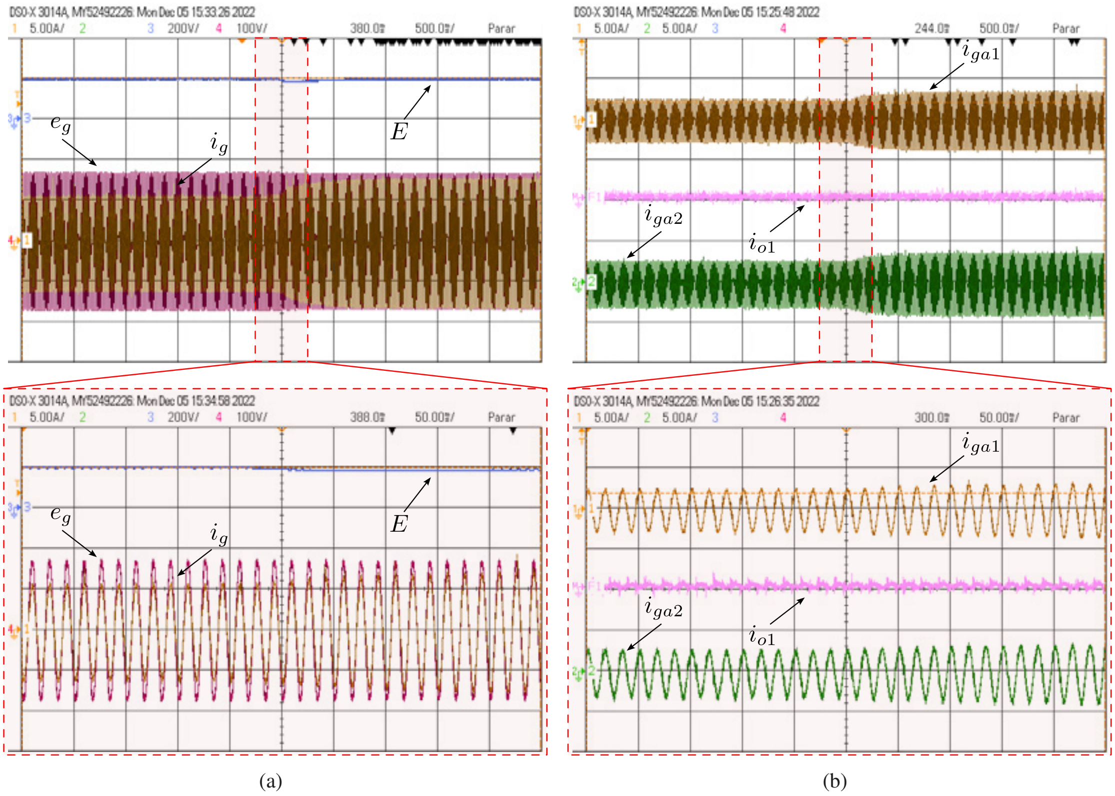

Fig. 18. Experimental results with load transient. (a) DC-link voltages E, current and voltage of grid e_g and i_g. (b) Internal currents of the rectifier A, $i_{g_{a1}}$, $i_{g_{a2}}$ and i_{o1}.

vol. 8, no. 2, pp. 1571–1583, Jun. 2020, doi:10.1109/JESTPE.2019.2906653.

[9] C. B. Jacobina, E. C. d. Santos Jr., N. Rocha, E. L. L. Fabrício, "Single-Phase to Three-Phase Drive System Using Two Parallel Single-Phase Rectifiers", *IEEE Transactions on Power Electronics*, vol. 25, no. 5,

pp. 1285–1295, May 2010, doi:10.1109/TPEL.2009.2037420.

[10] E. C. dos Santos, N. Rocha, C. B. Jacobina, "Suitable Single-Phase to Three-Phase AC–DC–AC Power Conversion System", *IEEE Transactions on Power Electronics*, vol. 30, no. 2, pp. 860–870, Feb. 2015, doi:10.1109/TPEL.2014.2308297.

[11] N. B. de Freitas, C. B. Jacobina, A. C. N. Maia, A. C. Oliveira, "Six-Leg Single-Phase to Three-Phase Converter", *IEEE Transactions on Industry Applications*, vol. 53, no. 6, pp. 5527–5538, Nov.–Dec 2017, doi:10.1109/TIA.2017.2720138.

[12] V. Verma, A. Kumar, "Cascaded Multilevel Active Rectifier Fed Three-Phase Smart Pump Load on Single-Phase Rural Feeder", *IEEE Transactions on Power Electronics*, vol. 32, no. 7, pp. 5398–5410, Jul. 2017, doi:10.1109/TPEL.2016.2605005.

[13] L. Zhang, K. Sun, Y. Xing, J. Zhao, "Parallel Operation of Modular Single-Phase Transformerless Grid-Tied PV Inverters With Common DC Bus and AC Bus", *IEEE Journal of Emerging and Selected Topics in Power Electronics*, vol. 3, no. 4, pp. 858–869, Dec. 2015, doi:10.1109/JESTPE.2015.2417196.

[14] L. Cheng, W. Wu, L. Qiu, X. Liu, J. Ma, J. Zhang, Y. Fang, "An improved data-driven based model predictive control for zero-sequence circulating current suppression in paralleled converters", *International Journal of Electrical Power & Energy Systems*, vol. 143, p. 108401, Dec. 2022, doi:https://doi.org/10.1016/j.ijepes.2022.108401.

[15] S. Vazquez, C. Montero, C. Bordons, L. G. Franquelo, "Model predictive control of a VSI with long prediction horizon", *in IEEE International Symposium on Industrial Electronics*, pp. 1805–1810, Jun. 2011, doi:10.1109/ISIE.2011.5984431.

[16] S. Kouro, P. Cortes, R. Vargas, U. Ammann, J. Rodriguez, "Model Predictive Control—A Simple and Powerful Method to Control Power Converters", *IEEE Transactions on Industrial Electronics*, vol. 56, no. 6, pp. 1826–1838, Jun. 2009, doi:10.1109/TIE.2008.2008349.

[17] D. Ramirez, M. E. Zarei, M. Gupta, J. Serrano, "Fast Model-based Predictive Control (FMPC) for grid connected Modular Multilevel Converters (MMC)", *International Journal of Electrical Power & Energy Systems*, vol. 119, p. 105951, Jul. 2020.

[18] M. Li, X. Wu, S. Huang, G. Liang, "Model predictive direct power control using optimal section selection for PWM rectifier with reduced calculation burden", *International Journal of Electrical Power & Energy Systems*, vol. 116, p. 105552, Mar. 2020.

[19] S. Vazquez, P. Acuna, R. P. Aguilera, J. Pou, J. I. Leon, L. G. Franquelo, "DC-Link Voltage-Balancing Strategy Based on Optimal Switching Sequence Model Predictive Control for Single-Phase H-NPC Converters", *IEEE Transactions on Industrial Electronics*, vol. 67, no. 9, pp. 7410–7420, Sept. 2020, doi:10.1109/TIE.2019.2941131.

[20] A. Lashab, D. Sera, J. M. Guerrero, "Model Predictive Control of Cascaded Multilevel Battery Assisted Quasi Z-Source PV Inverter with Reduced Computational Effort", *in IEEE Energy Conversion Congress and Exposition (ECCE)*, pp. 6501–6507, 2019, doi:10.1109/ECCE.2019.8912551.

[21] A. J. S. Filho, R. S. Inomoto, L. L. Rodrigues, R. B. A. Cunha, O. A. C. Vilcanqui, "Predictive Control Applied to a Boost Converter of a Photovoltaic System", *Journal of Control, Automation and Electrical Systems*, vol. 33, pp. 393–405, Sept. 2022, doi:https://doi.org/10.1007/s40313-021-00796-9.

[22] H. A. Young, M. A. Perez, J. Rodriguez, H. Abu-Rub, "Assessing finite-control-set model predictive control: A comparison with a linear current controller in two-level voltage source inverters", *IEEE Industrial Electronics Magazine*, vol. 8, no. 1, pp. 44–52, Mar. 2014.

[23] I. Harbi, J. Rodriguez, E. Liegmann, H. Makhamreh, M. L. Heldwein, M. Novak, M. Rossi, M. Abdelrahem, M. Trabelsi, M. Ahmed, P. Karamanakos, S. Xu, T. Dragičević, R. Kennel, "Model-Predictive Control of Multilevel Inverters: Challenges, Recent Advances, and Trends", *IEEE Transactions on Power Electronics*, vol. 38, no. 9, pp. 10845–10868, Sept. 2023, doi:10.1109/TPEL.2023.3288499.

[24] F. S. Guedes, N. Rocha, A. M. Maciel, A. J. S. Filho, "Finite-Set Model Predictive Direct Power Control for DFIG with Reduced Number of Voltage Vectors", *Brazilian Journal of Power Electronics*, vol. 28, pp. 63–73, Mar. 2023, doi:http://dx.doi.org/10.18618/REP.2023.1.0025.

[25] J. Rodriguez, S. Bernet, P. K. Steimer, I. E. Lizama, "A Survey on Neutral-Point-Clamped Inverters", *IEEE Transactions on Industrial Electronics*, vol. 57, no. 7, pp. 2219–2230, Jul. 2010, doi:10.1109/TIE.2009.2032430.

[26] W. Huang, W. Hua, Q. Fan, "Performance analysis and comparison of two fault-tolerant model predictive control methods for five-phase PMSM drives", *CES Transactions on Electrical Machines and Systems*, vol. 5, no. 4, pp. 311–320, Dec. 2021, doi:10.30941/CESTEMS.2021.00036.

[27] T. Geyer, N. Oikonomou, G. Papafotiou, F. Kieferndorf, "Model predictive pulse pattern control", *in IEEE Energy Conversion Congress and Exposition*, pp. 3306–3313, 2011, doi:10.1109/ECCE.2011.6064215.

[28] J. Lei, L. Tarisciotti, A. Trentin, P. Zanchetta, P. Wheeler, A. Formentini, "Fixed frequency finite-state model predictive control for indirect matrix converters with optimal switching pattern", *in IEEE Energy Conversion Congress and Exposition (ECCE)*, pp. 1–8, 2016, doi:10.1109/ECCE.2016.7855118.

[29] L. Tarisciotti, P. Zanchetta, A. Watson, J. C. Clare, M. Degano, S. Bifaretti, "Modulated Model Predictive Control for a Three-Phase Active Rectifier", *IEEE Transactions on Industry Applications*, vol. 51, no. 2, pp. 1610–1620, Mar.–Apr. 2015, doi:10.1109/TIA.2014.2339397.

[30] M. Rivera, M. Perez, V. Yaramasu, B. Wu, L. Tarisciotti, P. Zanchetta, P. Wheeler, "Modulated model predictive control (M2PC) with fixed switching frequency for an NPC converter", *in IEEE 5th International Conference on Power Engineering, Energy and Electrical Drives (POWERENG)*, pp. 623–628, 2015, doi:10.1109/PowerEng.2015.7266389.

[31] L. Tarisciotti, P. Zanchetta, A. Watson, P. Wheeler, J. C. Clare, S. Bifaretti, "Multiobjective Modulated Model Predictive Control for a Multilevel Solid-State Transformer", *IEEE Transactions on Industry Applications*, vol. 51, no. 5, pp. 4051–4060, Sept.–Oct 2015, doi:10.1109/TIA.2015.2429113.

[32] G. M. d. S. Rodrigues, N. Rocha, I. J. d. N. Silva, E. R. C. da Silva, V. F. M. Melo, "Modulated Predictive Controller for a Single-Phase Cascaded Transformer Multilevel Inverter", *in 12th Seminar on Power Electronics and Control (SEPOC 2019)*, 2019.

[33] F. Yu, K. Li, Z. Zhu, X. Liu, "An Over-Modulated Model Predictive Current Control for Permanent Magnet Synchronous Motors", *IEEE Access*, vol. 10, pp. 40391–40401, Apr. 2022, doi:10.1109/ACCESS.2022.3166511.

[34] M. Vijayagopal, P. Zanchetta, L. Empringham, L. de Lillo, L. Tarisciotti, P. Wheeler, "Control of a Direct Matrix Converter With Modulated Model-Predictive Control", *IEEE Transactions on Industry Applications*, vol. 53, no. 3, pp. 2342–2349, May–Jun. 2017, doi:10.1109/TIA.2017.2674602.

[35] A. Nasr, C. Gu, G. Buticchi, S. Bozhko, C. Gerada, "A Low-Complexity Modulated Model Predictive Torque and Flux Control Strategy for PMSM Drives Without Weighting Factor", *IEEE Journal of Emerging and Selected Topics in Power Electronics*, vol. 11, no. 2, pp. 1305–1316, Apr. 2023, doi:10.1109/JESTPE.2022.3152652.

[36] R. d. C. Ferreira, S. M. A. Dias, N. Rocha, E. R. C. d. Silva, V. F. M. B. Melo, "Modulated Predictive Controller for a Single-Phase to Three-Phase Converters with Two Parallel Single-Phase Rectifiers", *in Brazilian Power Electronics Conference (COBEP)*, pp. 1–8, 2021, doi:10.1109/COBEP53665.2021.9684073.

[37] S. Jean, *Contribution to the Robustication of Model Predictive Control Techniques for Electrical System Applications*, Ph.D. thesis, Université de Cergy Pontoise, Paris-France, 2016.

[38] S. S. Yeoh, T. Yang, L. Tarisciotti, C. I. Hill, S. Bozhko, P. Zanchetta, "Permanent-Magnet Machine-Based Starter–Generator System With Modulated Model Predictive Control", *IEEE Transactions on Transportation Electrification*, vol. 3, no. 4, pp. 878–890, Dec. 2017, doi:10.1109/TTE.2017.2731626.

[39] P. Cortes, J. Rodriguez, C. Silva, A. Flores, "Delay Compensation in Model Predictive Current Control of a Three-Phase Inverter", *IEEE Transactions on Industrial Electronics*, vol. 59, no. 2, pp. 1323–1325, Feb. 2012, doi:10.1109/TIE.2011.2157284.

[40] C. Lu, Z. Zhou, A. Jiang, M. Luo, P. Shen, Y. Han, "Comparative performance evaluation of phase-locked loop (PLL) algorithms for single-phase grid-connected converters", *in IEEE 8th International Power Electronics and Motion Control Conference (IPEMC-ECCE Asia)*, pp. 902–907, 2016, doi:10.1109/IPEMC.2016.7512406.

[41] I. Ben Ali, M. W. Naouar, E. Monmasson, "DC-link voltage control of a single-phase AFE rectifier with reactive power ancillary service", *in 6th IEEE International Energy Conference (ENERGYCon)*, pp. 216–221, 2020, doi:10.1109/ENERGYCon48941.2020.9236605.

[42] J. I. Leon, S. Vazquez, A. J. Watson, L. G. Franquelo, P. W. Wheeler, J. M. Carrasco, "Feed-Forward Space Vector Modulation for Single-Phase Multilevel Cascaded Converters With Any DC Voltage Ratio", *IEEE Transactions on Industrial Electronics*, vol. 56, no. 2, pp. 315–325, Feb. 2009, doi:10.1109/TIE.2008.926777.

BIOGRAPHIES

Ruben da Cruz Ferreira, was born in João Pessoa, Paraíba, Brazil, in 2000. He is a bachelor's student in electrical engineering from the Federal University of Paraíba, João Pessoa, Brazil. Since 2019, he is working in researches about shunt active power filters and power converters. His research interests include power electronics, renewable energy sources and electrical drives.

Sofia M. Almeida Dias, was born in João Pessoa, Paraíba, Brazil, in 1997. He received the B.S. and M.S. degrees in electrical engineering from the Federal University of Paraíba, João Pessoa, Brazil, in 2021 and 2023, respectively. Between 2017 and 2019, she worked with modeling and driving electrical machines, and between 2020 and 2023, he dedicated his studies to various PWM techniques and predictive control in variable speed systems. She currently works in the Nacional Operator of the Electric System (ONS) in the planning department.

Nady Rocha, was born in São Gabriel, Bahia, Brazil, in 1982. He received the B.S., M.S., and Ph.D. degrees in electrical engineering from the Federal University of Campina Grande, Campina Grande, Brazil, in 2006, 2008, and 2010, respectively. Since 2011, he has been with the Department of Electrical Engineering, Federal University of Paraíba, João Pessoa, where he is currently an Associate Professor of Electrical Engineering. His research interests include power electronics, renewable energy sources, and electrical drives.

Edison Roberto Cabral da Silva, received the B.S.E.E. degree from the Polytechnic School of Pernambuco, Recife, Brazil, in 1965, the M.S.E.E. degree from the University of Rio de Janeiro, Brazil, in 1968, and the Dr. Eng. degree from the University Paul Sabatier, Toulouse, France, in 1972. He was the Director of the Research Laboratory on Industrial Electronics and Machine Drives, LEIAM, Campina Grande, Brazil, for 30 years. He is currently Professor Emeritus at both University of Campina Grande, UFCG, and University of Paraiba, UFPB, where he is still acting. His current research work is in the area of power electronics and renewable energy systems. Co-author of the book entitled "Advanced Power Electronics Converters: PWM Converters Processing AC Voltages", IEEE/Wiley, he is a member of the Brazilian Society on Power Electronics, SOBRAEP (Honorable), Brazilian Society on Automatic Control, SBA, and IEEE (Life-Fellow). He is also a SBA Past-President.

Victor F. M. Bezerra Melo, was born in Pesqueira, Brazil, in 1988. He received the B.S., M.S., and Ph.D. degrees in electrical engineering from the Federal University of Campina Grande, Campina Grande, Brazil, in 2012, 2013, and 2017, respectively. From October 2014 to June 2018 he was with Federal Institute of Technology of Pernambuco (IFPE), Afogados da Ingazeira, Brazil, where he was a Professor. Since June 2018 he has been with the Renewable Energies Department, Federal University of Paraíba, where he is currently a Professor. His current research interests include power electronics, static converters, and electrical drives.